Transient Operational Characteristics of a Dual Compensation Chamber Loop Heat Pipe Without the Bayonet for Avionics Cooling

Lijun Chen, first author
School of Aeronautic Science and Engineering, Beihang University
Beijing 100191, China
cljzy2305514@buaa.edu.cn

Yongqi Xie, second author
School of Aeronautic Science and Engineering, Beihang University
Beijing 100191, China
xyq@buaa.edu.cn

Longzhu Han, third author[1]
School of Aeronautic Science and Engineering, Beihang University
Beijing 100191, China
hlz@buaa.edu.cn

Hongwei Wu, forth author
School of Physics, Engineering and Computer Science, University of Hertfordshire
Hatfield, AL10 9AB, UK
h.wu6@herts.ac.uk

Zhen Fang, fifth author
School of Aeronautic Science and Engineering, Beihang University
Beijing 100191, China
fangzz@buaa.edu.cn

[1] Corresponding author.

ABSTRACT

The removal of bayonet structures reduces the manufacturing complexity of loop heat pipes (LHPs). This study investigates the transient characteristics of a newly designed dual compensation chamber loop heat pipe (DCCLHP) without a bayonet in high acceleration fields and analyzes instability phenomena. This work was conducted under four typical installation orientations, accelerations of 3~15g, heat loads of 20~450 W, and heat sink temperatures of 15~25 ℃. Results demonstrate that the absence of the bayonet does not significantly degrade DCCLHP performance. Even at the unfavorable Orientation I, the system successfully starts up at 15g and 20 W while maintaining stable operation at 6g and 450 W. The acceleration direction significantly influences operational characteristics. Although favorable for liquid return, excessive acceleration may amplify the temperature difference between the two CCs, thereby elevating the evaporator temperature. Notably, the DCCLHP may maintain satisfactory performance under high heat loads at the unfavorable Orientation IV. Additionally, several instability phenomena are observed. Vapor-liquid redistribution may induce evaporator temperature rise in a period of time, and the acceleration magnitude alters the minimum heat load triggering this redistribution. Temperature oscillations occur only under specific conditions, with higher accelerations causing oscillatory behaviors. Temperature overshoot manifests mainly under lower heat loads and orientations favorable for liquid return, while increasing acceleration magnitude tends to weaken the overshoot. These findings provide critical data support and technical insights for the simplified design of DCCLHPs and their practical applications in aircraft.

***Keywords**: Aircraft; Thermal management; Loop heat pipe; Acceleration; Transient characteristics*

1. INTRODUCTION

Advanced aircraft are equipped with numerous highly integrated electronic devices with high heat flux. These components generate substantial heat within confined spaces, easily forming localized hot spots that impair normal operation [1, 2]. Traditional single-phase cooling technologies [3,4] exhibit insufficient heat dissipation capacity, while two-phase cooling methods such as spray cooling and jet impingement cooling [5, 6] impose stringent installation requirements. In contract, loop heat pipes (LHPs) offer high heat transfer efficiency, long-distance heat transport, and flexible design and installation [7–11], demonstrating unique advantages in thermal management solutions for onboard electronic devices [12, 13].

However, conventional single compensation chamber (CC) LHPs may fail to operate normally under unfavorable orientations in gravity field [14, 15], and they face even greater challenges in adapting to the hyper-gravity environments caused by aircraft acceleration variations during maneuvering flight [16]. To address the issue of insufficient capillary wick liquid supply due to adverse installation orientations, dual compensation chamber loop heat pipes (DCCLHPs) have been developed [17, 18].

To date, many researchers have investigated the operational performance of DCCLHPs under various installation orientations in gravity field. Lin et al. [19–21] early found that the DCCLHP with a bayonet could start up and operate normally at any orientation but exhibit large temperature overshoots under low heat loads. Through visualization techniques, they observed phenomena such as bubble formation, reverse flow, and liquid redistribution in the evaporator core caused by heat leakage during startup, and revealed unstable behaviors, including temperature oscillations and transient penetration of vapor. Feng et al. [22] specifically investigated instabilities in a DCCLHP with a bayonet, including temperature hysteresis. It was indicated that reverse flow was caused by elevated pressure from evaporation or vapor penetration in the evaporator core. Temperature oscillations occurred more easily when the bayonet-equipped CC was positioned above the evaporator. Zhao et al. [23] employed visualization methods to investigate the operating performance of a bayonet-equipped DCCLHP for wing de-icing. Results demonstrated that the angle of attack significantly affected both operating and condenser temperatures, potentially inducing system temperature oscillations. To enhance the startup performance of DCCLHPs at different orientations, Bai et al. [24, 25] designed and tested variants featuring either an extended bayonet or dual bayonets. Their results showed these designs improved startup under low heat loads (10 W) across various orientations. However, temperature oscillations and overshoot were observed during startup at favorable orientations with low heat loads, attributed to liquid presence in the vapor grooves. Yang et al. [26] investigated the operating performance of a bayonet-equipped DCCLHP featuring an eccentric ceramic wick. The results demonstrated its successful startup under six different orientations at 2 W, achieving 450 W heat transfer over 2.0 m. And system performance improved with decreasing temperature difference between the CCs. Fu et al. [27] developed a bayonet-equipped DCCLHP with dual vapor and liquid lines, it failed to start up under adverse orientations at heat loads of 40-100 W, and temperature overshoot and oscillations were observed during startup at all orientations under low heat loads. Subsequently, they proposed a sequential cooling CC design

that enabled successful startup at all orientations under 0-100 W heat loads [28]. Recently, they also designed a 1 kW high-capacity DCCLHP featuring three parallel vapor/liquid lines and a bayonet, demonstrating reliable startup across multiple orientations at 0-300 W heat loads without significant temperature overshoot [29].

However, acceleration experiments can better simulate the actual maneuvering flight conditions of aircraft. Thus, Ku et al. [30, 31] conducted pioneering performance tests on a miniature ammonia single CC LHP under 1.2-4.8g accelerations. It was found that the LHP could normally operate in all tests. However, acceleration altered operational temperatures and could induce instabilities. Subsequently, they [32, 33] developed a mathematical model predicting LHP operating temperatures in acceleration fields, attributing temperature variations to additional flow resistance induced by acceleration. Fleming et al. [34, 35] investigated the operational performance of a water single CC LHP with a bayonet and secondary wick under accelerations of 0-10g. It was indicated that dry-out was correlated with both heat load and acceleration. The evaporator heat transfer coefficient and thermal resistance were minimally affected by acceleration, but at high heat loads, wall superheat slightly increased with rising acceleration. Yerkes et al. [16, 36, 37] investigated the effects of steady periodic accelerations (0.5-10g) and phase-shifted periodic variations in heat load and acceleration on the operating performance of a water single CC LHP. The results demonstrated that acceleration variations could detrimentally affect LHP performance in many conditions. For DCCLHPs, Phillips et al. [38] conducted performance tests on a DCCLHP under evaporator-to-condenser acceleration (10g at the condenser) and demonstrated its stable operation under heat loads up to 620 W. Wang et al. [39, 40] investigated the effects of five different orientations on the operating performance of a 1 kW-capacity ammonia DCCLHP with a bayonet under both gravity and acceleration conditions (up to 8g). Their results indicated that mechanical effects altered the condensate film thickness in the condenser, thereby affecting condenser capacity and the temperature of liquid returning to the CCs. Xie et al. [41–45] conducted a series of studies on the operational performance of bayonet-equipped DCCLHPs with water or ammonia as working fluids under stable/varying acceleration fields up to 15g at different orientations. Using visualization techniques, they observed and explained acceleration-induced instability phenomena. Recently, they also investigated elevated acceleration effects on the performance of a novel dual-CC flat loop heat pipe [46].

A synthesis of the aforementioned references reveal that currently designed and studied DCCLHPs universally incorporate bayonet structures. Both the bayonet structure and secondary wick were originally developed to ensure effective liquid supply to the central portion of the wick, particularly for microgravity applications [47]. These designs have been continuously refined or remain in use today, primarily to enhance the startup performance of DCCLHPs [26,27]. Experimental evidence, however, indicates that bayonet-equipped LHPs may experience significant capillary force reduction under substantial heat leakage conditions [48], and could also lead to the CC overheating when operating with excessive working fluid mass charge, resulting in system failure [49]. On the other hand, removing the bayonet structure can simplify the manufacturing process of DCCLHPs and moderately reduce system mass.

Therefore, this study designed and fabricated a DCCLHP without a bayonet, aiming to investigate its operational performance and adaptability under high acceleration conditions, using ammonia as the working fluid. The research focuses on examining the effects of heat loads, orientations, acceleration magnitudes, and heat sink temperatures on the transient characteristics of the DCCLHP in acceleration fields, while analyzing and explaining the instability phenomena induced by acceleration effects. According to existing references, this work represents the first experimental investigation of the transient characteristics of a bayonet-free DCCLHP under acceleration conditions. The findings provide critical data support and technical guidance for both the practical application of DCCLHPs in high-speed aircraft and the design of simplified configurations.

2. Experimental setup and procedures

Fig. 1 presents the schematic diagram of the experimental system in this study, which primarily consists of the acceleration regulatory system, the heating control and data acquisition system, the cooling system, and the DCCLHP testing unit.

In this work, the newly designed DCCLHP comprises a cylindrical evaporator, two cylindrical CCs, a serpentine condenser, a vapor line, and a liquid line, with helical structure incorporated in the mid-portions of both transport lines. The schematic diagram of the internal structure of the evaporator and CCs is shown in Fig. 2. Unlike the conventional DCCLHP, this design eliminates the bayonet structure. The CC1 and CC2 are directly connected through the evaporator core, and the condensed working fluid enters the CC2 directly via the liquid line, which reduces manufacturing complexity and cost. The condenser tubing is welded onto

an aluminum plate. All shells are constructed from 316L stainless steel, and the capillary wick is fabricated by sintering nickel powder. Furthermore, since most onboard electronic devices require operational temperature below 75 ℃, ammonia was selected as the working fluid due to its high Dundar number, large dP/dT value, and low superheat requirement for boiling [50]. The working fluid charge mass was determined to be approximately 60 g based on the theoretical analysis in Reference [19]. Both excessively low and high working fluid charge can lead to difficulties in system startup, potentially resulting in insufficient liquid supply or temperature overshoot, respectively [19, 49]. The detailed design parameters of this DCCLHP are listed in Table 1.

As shown in Fig. 1, the DCCLHP is mounted inside the test enclosure at the end of the rotating arm. The centrifuge can provide a maximum radial centrifugal acceleration of 15g. To ensure the safety and stability of the experimental system, the test duration for each condition is typically limited to 60 minutes, which covers the time required for the DCCLHP to reach steady state under any condition in this study. A thin-film electric heater is attached to the exact center of the evaporator's outer surface. The heat input Q is regulated by a DC power supply, with its maximum value set to 450 W. The voltage (U) and current (I) measurement accuracies are ±0.1% and ±0.5%, respectively. The temperature variations at each measurement point on the DCCLHP were recorded using PT100 temperature sensors with an accuracy of ±0.3 ℃ and an Agilent 34970A data logger. The exact positions of all temperature measurement points are shown in Fig. 3. Specifically, CON_1, CON_3, and CON_5 are located at the bends of the condenser's serpentine tubing. The condenser was firmly secured to the aluminum cooling plate of the cooling system, with thermal grease applied at the interface to minimize contact thermal resistance. COLD_IN was used to monitor the cooling water temperature entering the cooling plate for stable heat sink temperature control. In this experiment, three heat sink temperature setpoints were adopted for specific operating conditions: 15 ℃, 20 ℃, and 25 ℃.

Fig. 4 presents the schematic diagrams of the four installation orientations of the DCCLHP and the corresponding internal vapor-liquid distributions in this study. The four orientations are labeled as Orientation I to IV. Arrows marked with a and g denote the directions of centrifugal acceleration and gravitational acceleration, respectively. The symbol ⊗ indicates gravitational acceleration directed inward, perpendicular to the plane of the page. Unless otherwise specified, all accelerations referenced in this text

refer specifically to centrifugal acceleration. As illustrated in Fig. 4, the vapor-liquid distribution of the working fluid differs in the two CCs due to the distinct force directions.

3. Results and discussion

3.1 Operating characteristics for different orientations under acceleration

3.1.1 Transient behaviors at Orientation I

Fig. 5 shows the temperature variations of the DCCLHP at Orientation I with the 20 ℃ heat sink temperature under different conditions, respectively corresponding to 6g and 20 W, 6g and 450 W, 15g and 20 W, 15g and 50 W. The DCCLHP can successfully start up at 20 W under the most unfavorable orientation, exhibiting operational temperatures of 28.1 ℃ and 33.0 ℃ under 6g and 15 g conditions, respectively. Furthermore, it demonstrated normal operation at 6g and a relatively high heat load of 450 W, maintaining a stable temperature of 43.3 ℃. However, at 15g and a low heat load of 50 W, the evaporator temperature continuously increased without reaching a steady state. Additionally, system stabilization time increased significantly at lower heat loads.

In Fig. 5(a), following the application of acceleration and heat load at 170 s, vapor gradually generated in the evaporator and flowed through the vapor line into the condenser. The temperatures at EVA, CC1, CC2, and VL_OUT increased, while all measurement points on the condenser showed gradual temperature rise. Concurrently, LL_IN and LL_OUT temperatures decreased sequentially as subcooled working fluid slowly entered the CC2, indicating the progressive establishment of a stable forward circulation. Ultimately, the temperatures of EVA, CC1, and CC2 kept at 28.1 ℃, 27.4 ℃, and 27.3 ℃, respectively. Due to its proximity to the CC2, LL_OUT maintained a higher temperature than LL_IN. The condenser operated with only partial utilization, as evidenced by the vapor-liquid interface being located between VL_OUT and CON_1. Under acceleration effects, vapor accumulation near CON_3 resulted in a locally high temperature. As illustrated in Fig. 5(c), at 15g and 20 W, the temperature evolution trends at all measurement points followed patterns similar to those observed in the aforementioned case. However, the stabilized temperatures of EVA, CC1, and CC2 reached 33.0 ℃, 31.1 ℃, and 31.2 ℃ respectively, exhibiting systematically higher values compared to the above condition.

As depicted in Fig. 5(b), upon application of the thermal-mechanical load at 65 s, vapor rapidly generated and entered the condenser, the temperatures of the evaporator, vapor line, and condenser sharply increased. The subcooled liquid pushed into the liquid line triggered a sharp sequential temperature drop at LL_IN and LL_OUT. With working fluid returning into the CC2, both CC1 and CC2 temperatures slightly decreased around 80 s before subsequently rising again. EVA, CC1, and CC2 reached steady temperatures of 43.3 ℃, 40.6 ℃, and 38.7 ℃, respectively. Although the CC1 and CC2 exhibited similar vapor-liquid distributions, the direct inflow of condensed working fluid into the CC2 resulted in its slightly lower temperature compared to the CC1. During stable operation, the condenser was in a complete two-phase state, with liquid accumulation near CON_1 and CON_5 due to acceleration effects, yielding their comparatively lower temperatures of 35.9 ℃ and 35.2 ℃.

In Fig. 5(d), after applying acceleration and heat load at 30 s, vapor slowly generated and entered the vapor line. The condenser temperature exhibited a slight increase, both LL_IN and LL_OUT temperatures decreased slightly. It was indicated that the condenser was barely utilized, as the vapor failed to undergo effective condensation, and the working fluid return flow encountered substantial flow resistance. Meanwhile, the temperatures at EVA, CC1, and CC2 continued to rise, suggesting increasing heat leakage from the evaporator to the CCs. Consequently, the system failed to reach a steady state. The experiment was terminated to prevent potential wick breakdown.

For the DCCLHP, the driving pressure Δp_{cap} generated by the capillary wick must exceed the total pressure drop of the loop for normal startup and operation. In this work, the Δp_{cap} must satisfy the following condition.

$$\Delta p_{\mathrm{cap}} \geq \Delta p_{\mathrm{vg}} + \Delta p_{\mathrm{vl}} + \Delta p_{\mathrm{con,v}} + \Delta p_{\mathrm{con,l}} + \Delta p_{\mathrm{ll}} + \Delta p_{\mathrm{w}} + \Delta p_{\mathrm{a}} \tag{1}$$

$$\Delta p_{\mathrm{a}} = \rho a l \tag{2}$$

Here, Δp_{vg} and Δp_{vl} are the vapor pressure drops in the vapor grooves and vapor line respectively, $\Delta p_{\mathrm{con,v}}$ and $\Delta p_{\mathrm{con,l}}$ are the vapor and liquid pressure drops in the condenser, Δp_{ll} is the working fluid pressure drop in the liquid line, and Δp_{w} is the liquid pressure drop through the capillary wick. Δp_{a} is primarily the additional pressure head induced by acceleration on the liquid working fluid. When the flow direction of the working fluid aligns with the acceleration direction, Δp_{a} assumes a negative value; conversely, it becomes positive. However, when the flow direction is perpendicular to the acceleration direction, Δp_{a} is negligible.

Where ρ is the liquid density, a is the magnitude of acceleration, and l is the effective flow length of the working fluid along the acceleration direction. In fact, both Δp_{vg} and Δp_{vl} are relatively low and can be neglected. The total pressure drop in the external loop is primarily governed by $\Delta p_{con,l}$, Δp_{ll}, Δp_{w}, and Δp_{a}. Due to the horizontal configuration of the DCCLHP, the gravitational influence is also negligible.

At Orientation I, when subjected to 15g acceleration, Δp_{a} was significantly larger compared to the 6g condition. Consequently, the Δp_{cap} likely failed to meet the requirement of Eq (1) at 50 W, the insufficient subcooling of the return fluid and persistently increasing heat leakage from the evaporator to the CCs caused the operation failure. However, as the heat load was reduced from 50 W to 20 W, the mass flow rate decreased, leading to a reduction in system flow resistance. And the subcooling degree of the returning liquid was sufficient to balance the heat leakage from the evaporator. Therefore, the DCCLHP can successfully start up and achieve stable operation at 15g and 20 W. In addition, due to the higher Δp_{a}, the operational temperature at 15g and 20 W was notably elevated compared to that under 6g and 20 W condition.

The present DCCLHP demonstrated successful startup at low heat loads (20 W) under the adverse Orientation I even without the bayonet. This capability may be attributed to enhanced wick performance, system structure, and filling ratio. Moreover, the operating temperature of this DCCLHP for Orientation I at 450 W and 6g was 43.3 ℃, which is close to the values for Orientation I at a lower heat load of 300 W with the accelerations of 5g and 7g in Reference [51]. These results indicate that a rationally structural simplification does not result in significant performance loss.

3.1.2 Transient behaviors at Orientation II

Fig. 6 presents the temperature variations of the DCCLHP for Orientation II and 150 W with a heat sink temperature of 20 ℃, comparing the transient behaviors between 3g and 15g conditions. It is seen that the acceleration magnitude significantly impacts the transient operation of the system. Under the aforementioned 15g condition, the working fluid distribution within the condenser exhibits a distinct vapor-liquid interface. The operational temperatures at 3g and 15g are 28.5 ℃ and 31.8 ℃, respectively.

In Fig. 6(a), after applying acceleration and heat load at 90 s, the temperatures of LL_IN and LL_OUT exhibited an immediate decline, reaching their minimum values at 110 s and 160 s, which confirmed the transit of subcooled working fluid through the liquid line into the CC2. The temperature at CC2 initially increased but subsequently decreased at 110 s under the effect of the returning subcooled liquid,

before rising again at 170 s. When the system reached steady-state operation, the temperatures of EVA, CC1, and CC2 kept at 28.5 ℃, 26.8 ℃, and 25.1 ℃, respectively. Under the acceleration, a significant amount of vapor accumulated in the CC1, resulting in its temperature being notably higher than that of CC2. During this process, the condenser operated entirely in a two-phase state, while vapor was also present in the liquid line, leading to high temperature at LL_IN.

As shown in Fig. 6(b), when the acceleration was increased to 15g, the temperature of the CC2 continuously decreased during system startup until stabilization due to the effect of the returning subcooled liquid. Meanwhile, the temperatures of CON_4 and CON_3 exhibited abrupt drops at 135 s and 200 s, respectively, followed by gradual recovery to the steady-state. In the end, the temperatures of EVA, CC1, and CC2 stabilized at 31.8 ℃, 31.2 ℃, and 23.1 ℃, respectively, while the vapor-liquid interface in the condenser remained fixed between CON_3 and CON_4.

For Orientation II at 150 W, as the acceleration was increased from 3g to 15g, a distinct vapor-liquid interface emerged in the condenser, accompanied by a reduction in the two-phase zone length. And the acceleration-induced pressure head Δp_a enhanced liquid return. However, the operational temperature of the DCCLHP increased by 3.3 ℃, while the temperature difference between the CC2 and CC1 surged from 1.7 ℃ to 8.1 ℃. It was demonstrated that under the above operating conditions, while the liquid working fluid could effectively return to the CC2 under high acceleration, reducing its temperature from 25.1 ℃ to 23.1 ℃, the acceleration effects critically impeded adequate wick wetting near the CC1 side. As a result, heat leakage from the evaporator to the CC1 intensified sharply, driving the temperature of CC1 rise to 31.2 ℃ and likely causing localized wick dry out or breakdown, ultimately degrading the DCCLHP's operating performance.

3.1.3 Transient behaviors at Orientation III

Fig. 7 displays the temperature variations of the DCCLHP for Orientation III and 6g with a heat sink temperature of 20 ℃, under the 30 W and 200 W conditions. The DCCLHP exhibits temperature overshoot at the 30 W condition, with operational temperatures of 25.2 ℃ and 30.7 ℃ for the aforementioned two cases.

In Fig. 7(a), following the application of thermal-mechanical load at 60 s, the temperature at LL_IN exhibited an immediate decrease, while all other measurement points showed a rapid temperature rise. This

confirmed the entry of subcooled working fluid into the liquid line and CC2. At 195 s, the temperatures of EVA, CC1, CC2, VL_OUT, and LL_OUT displayed a sudden and rapid decline. Notably, the evaporator temperature dropped from a maximum value of 26.1 ℃. Meanwhile, CON_1 exhibited a sharp temperature rise due to the rapid passage of high-temperature vapor. Subsequently, the system gradually reached a steady state, with the temperatures of EVA, CC1, and CC2 stabilizing at 25.2 ℃, 24.8 ℃, and 24.7 ℃, respectively. The vapor-liquid interface in the condenser remained positioned between CON_1 and CON_2. Additionally, the temperature at LL_OUT continuously increased prior to reaching its peak of 24.9 ℃, indicating that heat leakage from the evaporator to the CCs was significant during this stage. This sustained heat transfer prevented cooling at the liquid line outlet near the CC2, keeping LL_OUT's temperature consistently high. The specific causes of the aforementioned temperature overshoot will be detailed in Section 3.4.

As illustrated in Fig. 7(b), after the application of acceleration and heat load at 55 s, the sequential temperature drops at LL_IN and LL_OUT again signified the progressive inflow of subcooled liquid into the CC2. Around 60 s, the temperatures of EVA, CC1, and CC2 slightly decreased before resuming their ascent until system stabilization. Ultimately, the temperatures of EVA, CC1, and CC2 kept at 30.7 ℃, 29.4 ℃, and 29.5 ℃, respectively. High-temperature vapor entered the liquid line, while the condenser operated entirely in a vapor-liquid two-phase state. Under the acceleration, CON_3 exhibited the lowest temperature of 27.1 ℃ due to the accumulation of liquid working fluid.

Under the 30 W condition, the mass flow rate of the working fluid was relatively low, only a small portion of the condenser was utilized. Due to the limited subcooling of the returning liquid and heat leakage from the evaporator to the CCs, the temperatures of the CCs remained elevated, approaching that of the evaporator. When the heat load was 200 W, the mass flow rate increased significantly, and the condenser was fully utilized. However, the higher flow resistance in the external loop caused the evaporator temperature to rise. According to Eq (3), the average temperature difference between the evaporator and the CCs (approximately 1.4 ℃) was also greater than that observed at 30 W.

$$\Delta p = \Delta T \left(\frac{dp}{dT} \right)_{\text{sat}} = \Delta T \frac{\lambda}{\left(v_{\text{g}} - v_{\text{l}} \right) T} \tag{3}$$

Where, ΔT is the mean temperature difference between the evaporator and CCs, λ is the latent heat of the liquid, v_g and v_l are the specific volumes of vapor and liquid respectively, T is the average temperature of the evaporator and CCs, and Δp is the total pressure drop in the external loop.

3.1.4 Transient behaviors at Orientation IV

Fig. 8 depicts the temperature variations of the DCCLHP for Orientation IV and 6g with a heat sink temperature of 20 ℃, under heat loads of 50 W, 100 W, 150 W, and 200 W. The DCCLHP exhibited continuous evaporator temperature escalation at 50 W, ultimately leading to operation failure. However, the system maintained stable operation at higher heat loads, with corresponding operational temperatures of 25.4 ℃, 27.9 ℃, and 30.3 ℃ for the aforementioned conditions.

In Fig. 8(a), upon application of the thermal-mechanical load at 15 s, the temperatures at all measurement points increased gradually. At 400 s, the temperatures of LL_IN, CON_4, and CON_1 started to decline sequentially. By approximately 700 s, the temperature at VL_OUT began to drop rapidly, while LL_IN increased slowly. At 820 s, the temperature at LL_IN surged abruptly. It was indicated that high-temperature vapor from the CCs back flowed into the liquid line, simultaneously pushing subcooled liquid into the vapor line. At approximately 880 s, the temperatures of EVA, CC2, and LL_OUT had elevated to 46.0 ℃, 43.9 ℃, and 39.6 ℃, respectively, with no signs of stabilization. For safety, the experiment was terminated.

Under conditions of higher acceleration and lower heat loads at Orientation IV, the DCCLHP frequently failed to maintain stable operation. This was likely because the acceleration generated a significant Δp_a in the condenser, while the Δp_{cap} cannot overcome the high flow resistance in the external loop. As a result, the CCs failed to receive sufficient subcooled liquid, causing the temperatures of both the evaporator and CCs to rise continuously. The capillary wick broke down, allowing high-temperature vapor from the CC2 to backflow into the liquid line, resulting in operation failure.

As shown in Fig. 8(b), the system successfully started up with the return of subcooled liquid. Due to the acceleration effects of Orientation IV, the CC1 accumulated a significant volume of liquid working fluid, resulting in a noticeably lower temperature compared to CC2. Under heat loads of 100 W, 150 W, and 200 W, the steady-state temperatures of CC1 kept at 22.4 ℃, 23.5 ℃, and 24.4 ℃, respectively, while the temperature difference between the CC1 and CC2 progressively increased to 2.2 ℃, 3.5 ℃, and 4.9 ℃.

Similar to the operating characteristics observed at Orientation II, a larger temperature difference between the two CCs correlated with a higher evaporator temperature, indicating intensified thermal imbalance under these conditions. In addition, when the heat load exceeded 100 W, the condenser became fully utilized, and the liquid line inlet also exhibited a vapor-liquid two-phase state.

It was noteworthy that for 6g and 200 W, the system operational temperature at Orientation IV was slightly lower than that at Orientation III. Under the two conditions, both the condenser and liquid line entered a two-phase state, and the acceleration-induced Δp_a of the working fluid in the condenser may exhibit minimal variation. However, for Orientation IV, the condensed liquid entering the CC2 rapidly flowed through the evaporator core under acceleration, effectively wetting the capillary wick. This behavior may contribute to a reduction in operational temperature to some extent, thereby enhancing the system's thermal performance.

Furthermore, although compared to References [51, 52], this DCCLHP has difficulty in startup for Orientation IV at low heat loads, its operating temperatures under 6g and heat loads of 150 W and 200 W were 27.9 ℃ and 30.3 ℃, respectively, which are even lower than those for Orientation IV at 5g with 150 W and 200 W in Reference [51]. These results collectively indicate that the bayonet-free DCCLHP did not exhibit significant performance loss in acceleration field.

3.2 Vapor-liquid redistribution

For Orientation II, vapor-liquid redistribution occurs under specific operating conditions. Specifically, after system startup, the external loop transitions from an entirely two-phase state to one with a clear vapor-liquid interface, until reaching steady-state operation. Fig. 9 presents the temperature variation curves of the DCCLHP for Orientation II at 12g and 150 W with heat sink temperatures of 15 ℃, 20 ℃, and 25 ℃. The corresponding operational temperatures under these conditions are 28.7 ℃, 32.6 ℃, and 35.7 ℃, respectively.

In Fig. 9(a), after the application of acceleration and heat load at 230 s, vapor rapidly generated and drove the subcooled liquid sequentially through LL_IN and LL_OUT before entering the CC2, causing a successive temperature drop in all three points. After 350 s, all measurement points exhibited a rising temperature trend, with the external loop operating in a two-phase state. Approximately 635 s later, LL_IN, CON_6, LL_OUT, and CON_5 began to decline sequentially. At 1500 s, the vapor-liquid interface retreated

to between CON_4 and CON_5, with EVA at 30.2 ℃. After 1600 s, the temperature at CON_4 also began to decrease, while that of CON_3 first declined and then gradually increased. During this process, the temperature at EVA continuously increased. When the system reached steady-state operation, the temperatures of EVA, CC1, and CC2 were 32.6 ℃, 31.2 ℃, and 23.6 ℃, respectively. The vapor-liquid interface in the condenser stabilized between CON_3 and CON_4. The DCCLHP achieved its final stable operation only after multiple adjustments of the vapor-liquid interface in the external loop.

When the heat sink temperature increased to 25 ℃, as shown in Fig. 9(b), the temperatures of all measurement points rose upon the application of acceleration and heat load, with the external loop transitioning into a vapor-liquid two-phase state. After 470 s, the temperatures of LL_IN, CON_6, CON_5, and LL_OUT began to decrease sequentially, the vapor-liquid interface retreated to between CON_4 and CON_5. By approximately 630 s, the temperatures of CON_4 and CON_3 also started to decline successively, further pushing the vapor-liquid interface back to between CON_2 and CON_3. At 810 s, the temperature at CON_2 also began to decrease. During the aforementioned process, the temperatures of EVA, CC1, and VL_OUT continued to rise, while the utilization efficiency of the condenser gradually decreased. Heat leakage from the evaporator to the CC1 persistently increased, leading to a continuous temperature rise in both EVA and CC1. The maximum temperature recorded at EVA reached 39.1 ℃. After 1085 s, the condenser's utilization efficiency improved, leading to temperature rises in CON_2, CON_3, and CON_4, while the temperatures of EVA, CC1, VL_OUT, and CON_1 began to decline. Upon reaching a steady state, the evaporator temperature kept at 35.7 ℃, with the vapor-liquid interface in the condenser located between CON_3 and CON_4.

However, when the heat sink temperature was reduced to 15 ℃, as illustrated in Fig. 9(c), the vapor-liquid redistribution disappeared, and the system operated normally until reaching steady state. The lower the heat sink temperature, the stronger the condenser's cooling capacity becomes, making it difficult to be fully utilized at 150 W. However, as the heat sink temperature increases, the condenser may experience a complete transition to a vapor-liquid two-phase state during operation. This phenomenon demonstrates that vapor-liquid redistribution may be directly related to the condenser's heat transfer.

Based on the comprehensive experimental results, it has been determined that the occurrence of vapor-liquid redistribution is not random but follows certain predictable patterns. Fig. 10 illustrates the vapor-

liquid distribution states in the external loop under different conditions for Orientation II with a heat sink temperature of 20 ℃. For this DCCLHP, the external loop tended to transition entirely into a two-phase flow under conditions of high heat loads and low accelerations. Conversely, under low heat loads and high accelerations conditions, a distinct vapor-liquid interface became clearly observable in the external loop. The vapor-liquid redistribution in the external loop emerged with increasing heat load, typically occurring when the condenser approached full utilization. Furthermore, higher acceleration elevated the minimum heat load required to achieve complete condenser utilization.

For Orientation II, the acceleration acts as a driving force for liquid flow in the condenser and a resisting force in the evaporator core, with the overall effect being a resistance. According to Eqs (1) and (2), the Δp_{cap} rises as the acceleration increases from 3g to 15g. Consequently, the ΔT between the evaporator and the CCs increases according to Eq. (3), causing in the higher operating temperature. Meanwhile, the condensation temperature rises, decreasing the temperature difference for condensation heat transfer. When the heat dissipation is constant, the required condensation area or the condensation length decreases, the vapor-liquid redistribution occurs. During the redistribution process, high transient operating temperature may occur, as shown in Fig. 9(b).

3.3 Temperature oscillation

Fig. 11 displays the temperature oscillation curves of the DCCLHP for Orientation III at 9g and 50 W with a heat sink temperature of 20 ℃. Upon applying acceleration and heat load at 60 s, vapor rapidly generated and entered the condenser, causing immediate temperature increases at all measurement points except LL_IN, along with a sharp rise in condenser utilization efficiency. Approximately 300 s later, temperature decreases were observed at the evaporator, CCs, vapor line, liquid line outlet, and condenser inlet sections, while other measurement point temperatures increased. This indicated further improvement in condenser utilization efficiency, resulting in increased subcooling of the returning working fluid. The enhanced subcooling effectively mitigated heat leakage from the evaporator to the CCs, thereby suppressing further temperature rises in both the evaporator and CCs. Subsequently, the system began to exhibit periodic temperature oscillations, with operating temperatures fluctuating between approximately 24.4 ℃ and 24.8 ℃.

The temperature oscillations are intrinsically linked to heat leakage from the evaporator to the CCs under acceleration effects, which induces periodic oscillations of the vapor-liquid interface within the

external loop. Under sustained heat load, the temperature at EVA increases, elevating the temperatures of VL_OUT, CON_1, and CON_2 with high-temperature vapor entering the condenser. Simultaneously, heat leakage from the evaporator increases the temperature of the CCs, where high-temperature vapor forces the working fluid back into the condenser. This shifts the vapor-liquid interface toward the condenser inlet, reducing temperatures of CON_3 to CON_5 while increasing those of LL_IN and LL_OUT. However, elevated pressure in the vapor line drives the vapor-liquid interface toward the condenser outlet, raising temperatures of CON_3 to CON_5, while subcooled working fluid reduces liquid line temperature. When the subcooled liquid returns to the CCs, the temperatures of the CCs and evaporator decrease, lowering the generated vapor temperature. This cycle repeats periodically. Notably, Orientation III facilitates working fluid return, further preventing excessive temperature rise in the evaporator. Therefore, while temperature oscillation manifests instability, it also represents a self-regulating behavior of the DCCLHP under certain operating conditions.

Fig. 12 shows the temperature variation curves of the DCCLHP for Orientation IV at 150 W with a heat sink temperature of 20 ℃, tested under acceleration conditions of 3g, 9g, 12g, and 15g. The corresponding operational temperatures are approximately 27.8 ℃, 27.8 ℃, 28.0 ℃, and 28.5 ℃, respectively. This indicates that as acceleration increases, the return flow resistance of the liquid working fluid rises, leading to a slight elevation in operational temperature. Moreover, the external loop maintains a two-phase state across these conditions without a distinct vapor-liquid interface.

When the acceleration increased from 9g to 12g, temperature oscillations with a period of approximately 290 s occurred across all measurement points except the CC1, which was nearly filled with liquid. The amplitude was about 0.4 ℃ at EVA, while LL_IN exhibited the largest fluctuation of 2.2 ℃. A distinct phase shift was observed between LL_IN and other measurement points, and periodic movement of the vapor-liquid interface occurred between CON_4 and LL_OUT. When the acceleration further increased to 15g, the temperature oscillations intensified, exhibiting a reduced period of 240 s. The amplitude reached about 0.5 ℃ at EVA, while LL_IN still showed the most pronounced fluctuation of 3.4 ℃. The vapor-liquid interface moves between CON_5 and LL_OUT. At 15g, a larger additional resistance is generated, which requires a greater capillary force than at 12g to balance the external loop resistance. As a result, the operating temperature at 15g is higher. Due to the larger subcooling of the returning liquid from the condenser at 15g,

the amplitude of temperature oscillation at LL_IN is greater than at 12g. Simultaneously, the additional resistance caused by the acceleration slightly reduces the period of system oscillations. For Orientation IV, while increased acceleration has a minimal impact on the system's operational temperature, it induces significant temperature oscillations. Such fluctuations are detrimental to electronic devices requiring stringent thermal stability.

3.4 Temperature overshoot

In this study, temperature overshoot predominantly occurs under low heat load conditions at Orientation II and III. Fig. 13 depicts the temperature variation curves of the DCCLHP for Orientation II under 30 W low heat load and 3g, 12g, and 15g acceleration conditions with a heat sink temperature of 20 ℃. It can be observed that under the 3g and 12g conditions, the system exhibits significant temperature overshoot during startup. The operational temperatures for the three conditions are 23.2 ℃, 23.8 ℃, and 24.2 ℃, respectively. The sharp increase in acceleration for Orientation II still raises the evaporator temperature, consistent with the conclusions in Section 3.1.2.

In Fig. 13(a), after the application of acceleration and heat load, vapor rapidly formed and entered the vapor line, causing a sharp temperature rise in VL_OUT. At approximately 230 s, the temperatures of EVA, CC1, CC2, and LL_OUT all reached their peak values of 24.6 ℃, 24.1 ℃, 23.4 ℃, and 23.5 ℃, respectively. This indicated significant heat leakage from the evaporator to the CCs, particularly to the CC1. After 230 s, the temperatures of these five points began to decline. The temperature rise rates at CON_1 and CON_2 accelerated, while the temperature difference between CON_2 and CON_3 significantly increased. This enhancement in condenser utilization led to improved subcooling of the returning working fluid. Consequently, the temperatures of both the evaporator and CCs decreased. When the system reached steady-state operation, the temperatures of EVA, CC1, and CC2 kept at 23.2 ℃, 23.0 ℃, and 22.8 ℃ respectively, with a temperature overshoot of 1.4 ℃ observed during the transient phase. Finally, the temperature at LL_OUT decreased to approach that of the condenser. The vapor-liquid interface in the condenser stabilized between CON_2 and CON_3.

Fig. 13(b) demonstrates similar temperature evolution characteristics in the DCCLHP to those observed in Fig. 13(a). At approximately 325 s, the temperatures of both EVA and CC1 peaked at 24.0 ℃ and 23.8 ℃ respectively. Subsequently, the temperatures of EVA, CC1, CC2, VL_OUT, and LL_OUT began

to decline, while CON_1 and CON_2 exhibited a rapid temperature rise. The condenser utilization efficiency increased sharply. At steady-state operation, the temperatures of EVA, CC1, and CC2 kept at 23.8 ℃, 23.6 ℃, and 23.3 ℃, respectively, with a temperature overshoot of 0.2 ℃. As shown in Fig. 13(c), when the acceleration increased to 15g, the operating process remained similar to the aforementioned scenario, but temperature overshoot was nearly negligible. At steady state, the temperatures of EVA, CC1, and CC2 kept at 24.2 ℃, 23.8 ℃, and 23.3 ℃, respectively.

It is indicated that the temperature overshoot is closely related to the heat leakage of the evaporator and thermal equilibrium of the CCs at low heat loads. For Orientation II at the same heat load, the increase in acceleration promotes the return flow of subcooled working fluid, thereby supplying more cooling capacity to the CCs. It reduces the temperature rise caused by heat leakage from the evaporator to the CCs, consequently diminishing the temperature overshoot. Simultaneously, higher acceleration leads to a slight increase in operational temperature, accompanied by an enlarged temperature difference between the two CCs.

As shown in Fig. 14, for Orientation III at 30 W and 12g with a heat sink temperature of 20 ℃, the temperature variation trend of the DCCLHP is similar to that of the 6g condition corresponding to Fig. 7(a). Under 12g acceleration, when the system reached steady-state operation, the EVA temperature stabilized at 24.9 ℃ with a temperature overshoot of approximately 0.1 ℃, which was significantly lower than the 0.9 ℃ under the 6g condition. It is evident that for both Orientation II and III, favorable for working fluid return, higher accelerations consistently reduce the system's temperature overshoot. This mitigation effect decreases the adverse impact of excessive startup overshoot on precision electronic devices.

4. Conclusion

This study investigates the effects of heat loads, installation orientations, acceleration magnitudes, and heat sink temperature on the transient operational characteristics of a newly designed DCCLHP without a bayonet. It further examines the impact of acceleration on vapor-liquid redistribution, temperature oscillation, and temperature overshoot, yielding several key conclusions.

(1) This DCCLHP demonstrates competent performance despite the absence of a bayonet structure. It achieves successful startup at 15g and 20 W while maintaining stable operation at a relatively lower acceleration of 6g combined with a higher heat load of 450 W under the unfavorable Orientation I.

(2) Acceleration direction significantly influences operational characteristic. For Orientation II, increasing acceleration enhances working fluid return but may lead to wick end dry-out and greater heat leakage. For Orientation IV, the system exhibits startup difficulty with reverse flow at low heat loads but stable operation at higher heat loads, where the bayonet-free design may improve wick wettability, achieving performance comparable to Orientation III.

(3) The operating temperature increases with heat load or acceleration rising, accompanied by a greater temperature difference between the two CCs, at Orientation II and IV.

(4) The vapor-liquid redistribution occurs during the transitional phase when the condenser approaches full utilization with increasing heat load, during which elevated operating temperature may arise. This phenomenon results from thermodynamic instabilities under acceleration effects. Furthermore, increasing acceleration raises the minimum heat load required to achieve complete condenser utilization.

(5) Temperature oscillation occurs only at low heat loads for Orientation III and at relatively high heat loads for Orientation IV. For Orientation IV at 150 W, elevated acceleration induces temperature oscillations. The fluctuation period decreases from 290 s at 12g to 240 s at 15g, while the temperature amplitude at LL_IN increases from 2.2 ℃ (12g) to 3.4 ℃ (15g). Notably, the evaporator temperature amplitude remains nearly identical under the two acceleration conditions.

(6) At orientations favoring working fluid return (e.g., Orientations II and III), the system exhibits temperature overshoot at low heat loads, primarily attributed to heat leakage from the evaporator to the CCs. However, appropriately increasing acceleration magnitude effectively reduces the temperature overshoot, thereby mitigating its adverse effects on electronic devices. To illustrate, for Orientation II at 30 W, the overshoot values at 3g, 12g, and 15g are 1.4 ℃, 0.2 ℃, and nearly 0 ℃, respectively.

ACKNOWLEDGMENT

Due to submission requirements, it is not disclosed temporarily.

FUNDING

The work presented in this paper was supported by the National Natural Science Foundation of China (NSFC).

NOMENCLATURE

I	Current, [A]
Q	Heat load, [W]
T	Temperature, [°C]
U	Voltage, [V]
a	Centrifugal acceleration, [m/s^2]
g	Gravitational acceleration, [9.81 m/s^2]
l	Length, [m]
p	Pressure, [Pa]
v	Specific volume of working fluid, [m^3/kg]

Greek symbols

ρ	Density, [kg/m^3]
λ	Latent heat, [kJ/kg]

Subscripts

a	Centrifugal acceleration
cap	Capillary pressure
con,l	Liquid pressure drop in the condenser
con,v	Vapor pressure drop in the condenser
g	The specific volume of vapor

l	The specific volume of liquid
ll	Liquid line
sat	Saturation
vg	Vapor groove
vl	Vapor line
w	Wick

Abbreviations

CC	Compensation chamber
DCCLHP	Dual compensation chamber loop heat pipe
ID	Inside diameter
LHP	Loop heat pipe
OD	Outside diameter

531
532

REFERENCES

[1] Sun, B., and Li, J., 2024, "Toward extremely low thermal resistance with extremely low pumping power consumption for ultra-high heat flux removal on chip size scale." Energ. Convers. Manage., **306**, p. 118293. DOI: 10.1016/j.enconman.2024.118293

[2] Li, C., Su, L., and Chen, Q., 2025, "Prediction of flow boiling characteristics in manifold microchannel radiator based on high heat flux cooling." Int. J. Therm. Sci., **210**, p. 109554. DOI: 10.1016/j.ijthermalsci.2024.109554

[3] Khalaj, A. H., and Halgamuge, S. K., 2017, "A Review on efficient thermal management of air-and liquid-cooled data centers: From chip to the cooling system." Appl. Energy, **205**, pp. 1165-1188. DOI: 10.1016/j.apenergy.2017.08.037

[4] Zhang, C., Wang, H., and Huang, Y., 2025, "Immersion liquid cooling for electronics: Materials, systems, applications and prospects." Sust. Energ. Rev., **208**, p. 114989. DOI: 10.1016/j.rser.2024.114989

[5] Zhou, N., Tang, G., and Liu, Y., 2024, "Experimental Investigation on Spray Cooling Heat Transfer Properties of Ethylene Glycol− Water-Based Nanofluids." ASME J. Therm. Sci. Eng. Appl., **16**(10). DOI: 10.1115/1.4066176

[6] Fawaz, H. E., Osama, M. M., and Maghrabie, H. M., 2024, "Artificial neural networks application on average and stagnation Nusselt number prediction for impingement cooling of flat plate with helically coiled air jet." ASME J. Therm. Sci. Eng. Appl., **16**(2). DOI: 10.21203/rs.3.rs-3304473/v1

[7] Maydanik, Y. F., 2005, "Loop heat pipes." Appl. Therm. Eng., **25**(5-6), pp. 635-657. DOI: 10.1016/j.applthermaleng.2004.07.010

[8] Bai, L., Fu, J., and Lin, G., 2019, "Quiet power-free cooling system enabled by loop heat pipe." Appl. Therm. Eng., **155**, pp. 14-23. DOI: 10.1016/j.applthermaleng.2019.03.147

[9] Domiciano, K. G., Krambeck, L., and Mantelli, M. B. H., 2025, "Development of thin loop heat pipe for compact electronics." Exp. Therm. Fluid Sci., p. 111510. DOI: 10.1016/j.expthermflusci.2025.111510

[10] Zhang, Y., Wang, G., and Wang, X., 2025, "Performance and energy consumption study of a dual-evaporator loop heat pipe for chip-level cooling." Appl. Therm. Eng., **258**, p. 124757. DOI: 10.1016/j.applthermaleng.2024.124757

[11] Nashine, C., Pandey, M., and Baraya, K. K., 2025, "Experimental studies on the transient characteristics and start-up behavior of a miniature loop heat pipe." Appl. Therm. Eng., **259**, p. 124814. DOI: 10.1016/j.applthermaleng.2024.124814

[12] Zilio, C., Righetti, G., and Mancin, S., 2018, "Active and passive cooling technologies for thermal management of avionics in helicopters: Loop heat pipes and mini-Vapor Cycle System." Therm. Sci. Eng. Prog., **5**, pp. 107-116. DOI: 10.1016/j.tsep.2017.11.002

[13] Wang, H., Lin, G., and Qin, H., 2023, "Design and experimental validation of a high capacity loop heat pipe for avionics cooling." Therm. Sci. Eng. Prog., **45**, p. 102139. DOI: 10.1016/j.tsep.2023.102139

[14] Chen, Y., Groll, M., and Mertz, R., 2005, "Steady-state and transient performance of a miniature loop heat pipe." *International Conference on Nanochannels, Microchannels, and Minichannels*, **41855**, pp. 183-189. DOI: 10.1115/ICMM2005-75122

[15] Bai, L., Lin, G., and Zhang, H., 2014, "Effect of evaporator tilt on the operating temperature of a loop heat pipe without a secondary wick." Int. J. Heat Mass Transf., **77**, pp. 600-603. DOI: 10.1016/j.ijheatmasstransfer.2014.05.044

[16] Yerkes, K. L., Scofield, J., and Courson, D., 2016, "Performance of a loop heat pipe subjected to a phase-coupled heat input to an acceleration field." *46th AIAA Thermophysics Conference*, p. 4145. DOI: 10.2514/6.2016-4145

[17] Gerhart, C., and Gluck, D., 1999, "Summary of operating characteristics of a dual compensation chamber loop heat pipe in gravity." *11th International Heat Pipe Conference*, Tokyo, Japan.

[18] Gluck, D., Gerhart, C., and Stanley, S., 1999, "Characterization of a high capacity, dual compensation chamber loop heat pipe." *AIP Conference Proceedings. American Institute of Physics*, **458**(1), pp. 943-948. https://pubs.aip.org/aip/acp/article-abstract/458/1/943/580702

[19] Lin, G., Zhang, H., and Shao, X., 2006, "Development and test results of a dual compensation chamber loop heat pipe." J. Thermophys. Heat Transf., **20**(4), pp. 825-834. DOI: 10.2514/1.21858

[20] Bai, L., Lin, G., and Wen, D., 2009, "Experimental investigation of startup behaviors of a dual compensation chamber loop heat pipe with insufficient fluid inventory." Appl. Therm. Eng., **29**(8-9), pp. 1447-1456. DOI: 10.1016/j.applthermaleng.2008.06.019

[21] Lin, G., Li, N., and Bai, L., 2010, "Experimental investigation of a dual compensation chamber loop heat pipe." Int. J. Heat Mass Transf., **53**(15-16), pp. 3231-3240.
DOI: 10.1016/j.ijheatmasstransfer.2010.03.003
[22] Feng, J., Lin, G., and Bai, L., 2009, "Experimental investigation on operating instability of a dual compensation chamber loop heat pipe." Sci. China Ser. E, **52**(8), pp. 2316-2322.
DOI: 10.1007/s11431-008-0285-4#citeas
[23] Zhao, Y., Chang, S., and Yang, B., 2017, "Experimental study on the thermal performance of loop heat pipe for the aircraft anti-icing system." Int. J. Heat Mass Transf., **111**, pp. 795-803.
DOI: 10.1016/j.ijheatmasstransfer.2017.04.009
[24] Bai, L., Tao, Y., and Guo, Y., 2020, "Startup characteristics of a dual compensation chamber loop heat pipe with an extended bayonet tube." Int. J. Heat Mass Transf., **148**, p. 119066.
DOI: 10.1016/j.ijheatmasstransfer.2019.119066
[25] Bai, L., Fu, J., and Pang, L., 2020, "Experimental study on a dual compensation chamber loop heat pipe with dual bayonet tubes." Appl. Therm. Eng., **180**, p. 115821. DOI: 10.1016/j.applthermaleng.2020.115821
[26] Yang, P., Yang, T., and Gao, T., 2023, "Experimental study on a dual compensation chamber loop heat pipe with a ceramic wick." Appl. Therm. Eng., **230**, p. 120750. DOI: 10.1016/j.applthermaleng.2023.120750
[27] Fu, J., Bai, L., and Zhang, Y., 2023, "Experimental study on the thermal performance of a dual compensation chamber loop heat pipe with dual vapor and condenser lines." Therm. Sci. Eng. Prog., **43**, p. 101994. DOI: 10.1016/j.tsep.2023.101994
[28] Fu, J., Bai, L., and Zhang, Y., 2024, "Improved startup performance of a dual compensation chamber loop heat pipe by sequential cooling to the compensation chambers." Int. J. Heat Mass Transf., **233**, p 126046.
DOI: 10.1016/j.ijheatmasstransfer.2024.126046
[29] Fu, J., Bai, L., and Zhang, Y., 2025, "Thermal performance of a kW-level long distance loop heat pipe with an air-cooling condenser." Int. J. Heat Mass Transf., **247**, p. 127145.
DOI: 10.1016/j.ijheatmasstransfer.2025.127145
[30] Ku, J., Ottenstein, L., and Kaya, T., 2000, "Testing of a loop heat pipe subjected to variable accelerating forces, Part 1: Start-up." SAE Technical Paper. DOI: 10.4271/2000-01-2488
[31] Ku, J., Ottenstein, L., and Kaya, T., 2000, "Testing of a loop heat pipe subjected to variable accelerating forces, Part 2: Temperature stability." SAE Technical Paper. DOI: 10.4271/2000-01-2489
[32] Kaya, T., and Ku, J., 2003, "Thermal operational characteristics of a small-loop heat pipe." J. Thermophys. Heat Transf., **17**(4), pp. 464-470. DOI: 10.2514/2.6805
[33] Kaya, T., and Ku, J., 2003, "Experimental investigation of performance characteristics of small loop heat pipes." *41st Aerospace Sciences Meeting and Exhibit*, p. 1038. DOI: 10.2514/6.2003-1038
[34] Fleming, A. J., Leland, Q. H., and Yerkes, K. L., 2016, "Aircraft thermal management using loop heat pipes: Experimental simulation of high acceleration environments using the centrifuge table test bed." Aircraft Thermal Management: Systems Architectures, **177**, p. 77.
[35] Fleming, A. J., Thomas, S. K., and Yerkes, K. L., 2010, "Titanium-water loop heat pipe operating characteristics under standard and elevated acceleration fields." J. Thermophys. Heat Transf., **24**(1), pp. 184-198. DOI: 10.2514/1.45684
[36] Yerkes, K., Scofield, J., and Courson, D., 2012, "An experimental investigation into the transient performance of a titanium-water loop heat pipe subjected to a steady-periodic acceleration field." *50th AIAA Aerospace Sciences Meeting including the New Horizons Forum and Aerospace Exposition*, p. 1009.
DOI: 10.2514/6.2012-1009
[37] Yerkes, K. L., Scofield, J. D., and Courson, D. L., 2014, "Steady-periodic acceleration effects on the performance of a loop heat pipe." J. Thermophys. Heat Transf., **28**(3), pp. 440-454. DOI: 10.2514/1.T3900
[38] Phillips, A., Fale, J., and Gernert, N., 1998, "Loop heat pipe qualification for high vibration and high-g environments." *36th AIAA Aerospace Sciences Meeting and Exhibit*, p. 885. DOI: 10.2514/6.1998-885
[39] Wang, H., Lin, G., and Guo, Y., 2024, "Experimental study of a high-capacity dual compensation chamber loop heat pipe at different orientations." Int. J. Therm. Sci., **202**, p. 109051.
DOI: 10.1016/j.ijthermalsci.2024.109051
[40] Wang, H., Lin, G., and Guo, Y., 2024, "Experimental investigation on the performance of a high capacity dual compensation chamber loop heat pipe under the effect of acceleration." Case Stud. Therm. Eng., **61**, p. 105013. DOI: 10.1016/j.csite.2024.105013
[41] Fang, Z., Xie, Y., and Xu, Y., 2021, "Performance investigation of a loop heat pipe integrated with thermoelectric cooler under acceleration field." Int. J. Heat Mass Transf., **178**, p. 121476.
DOI: 10.1016/j.ijheatmasstransfer.2021.121476

644 [42] Xie, Y., Li, X., and Han, L., 2020, "Experimental study on operating characteristics of a dual
645 compensation chamber loop heat pipe in periodic acceleration fields." Appl. Therm. Eng., **176**, p. 115419.
646 DOI: 10.1016/j.applthermaleng.2020.115419
647 [43] Lv, X., Xie, Y., and Zhang, H., 2021, "Temperature oscillation of a dual compensation chamber loop
648 heat pipe under acceleration conditions." Appl. Therm. Eng., **198**, p. 117450.
649 DOI: 10.1016/j.applthermaleng.2021.117450
650 [44] Xie, Y., Fang, Z., Zhang, H., 2022, "Visualization study on operating performance of a dual
651 compensation chamber loop heat pipe under acceleration condition." Appl. Therm. Eng., **217**, p. 119157.
652 DOI: 10.1016/j.applthermaleng.2022.119157
653 [45] Xie, Y., Pu, W., and Liu, S., 2024, "Visualized experimental study on steady-state performance of a
654 loop heat pipe under elevated acceleration fields." Appl. Therm. Eng., **238**, p. 121984.
655 DOI: 10.1016/j.applthermaleng.2023.121984
656 [46] Fang, Z., Xie, Y., and Wei, J., 2025, "Experimental study on the operating performance of a novel flat
657 loop heat pipe with liquid channels under terrestrial and accelerated conditions." Therm. Sci. Eng. Prog., **61**,
658 p. 103532. DOI: 10.1016/j.tsep.2025.103532
659 [47] Pastukhov, V. G., Maidanik, Y. F., and Fershtater, Y. G., 1997, "Adaptation of loop heat pipes to zero-
660 g conditions." *Sixth European Symposium on Space Environmental Control Systems*, **400**, p. 385.
661 https://adsabs.harvard.edu/full/1997ESASP.400..385P
662 [48] Van, Oost. S., Mullender, B., and Bekaert, G., 2002, "Secondary wick operation principle and
663 performance mapping in LHP and FLHP evaporators." *AIP conference proceedings. American Institute of*
664 *Physics*, **608**(1), pp. 94-103. DOI: 10.1063/1.1449713
665 [49] Adoni, A. A., Ambirajan, A., and Jasvanth, V. S., 2009, "Effects of mass of charge on loop heat pipe
666 operational characteristics." J. Thermophys. Heat Transf., **23**(2), pp. 346-355. DOI: 10.2514/1.41618
667 [50] Edison, T. A., Sengers, J. V., 1999, "Thermodynamic properties of ammonia in the critical region." Int.
668 J. Refrig., **22**(5), pp. 365-378. DOI: 10.1016/S0140-7007（99）00003-1
669 [51] Xie, Y., Zhang, J., Xie, L., Yu, Y., Wu, H., Zhang, H., and Gao, H., 2015, "Experimental investigation
670 on the operating characteristics of a dual compensation chamber loop heat pipe subjected to acceleration
671 field." Appl. Therm. Eng., **81**, pp. 297-312. DOI: 10.1016/j.applthermaleng.2015.02.014
672 [52] Xie, Y., Zhou, Y., Wen, D., Wu, H., Haritos, G., and Zhang, H., 2018, "Experimental investigation on
673 transient characteristics of a dual compensation chamber loop heat pipe subjected to acceleration forces."
674 Appl. Therm. Eng., **130**, pp. 169-184. DOI: 10.1016/j.applthermaleng.2017.11.014
675

676
677
678

Figure Captions List

Fig. 1 The schematic diagram of the experimental system

Fig. 2 Schematic diagram of the internal structure of the evaporator and CCs

Fig. 3 Schematic diagram of temperature measurement point arrangement

Fig. 4 Schematic diagram of installation orientations and corresponding vapor-liquid distributions

Fig. 5 Temperature variation curves of the 6g and 15g conditions at Orientation I with a heat sink temperature of 20 ℃

Fig. 6 Temperature variation curves of the 3g and 15g conditions for Orientation II at 150 W with a heat sink temperature of 20 ℃

Fig. 7 Temperature variation curves of the 6g conditions for Orientation III at 30 W and 200 W with a heat sink temperature of 20 ℃

Fig. 8 Temperature variation curves of the 6g conditions at Orientation IV with a heat sink temperature of 20 ℃

Fig. 9 Temperature variation curves of the 12g and 150 W conditions at Orientation II with different heat sink temperatures

Fig. 10 Vapor-liquid distribution states of the external loop under different conditions for Orientation II with a heat sink temperature of 20 ℃

Fig. 11 Temperature oscillation curves of the DCCLHP for Orientation III at 9g and 50 W with a heat sink temperature of 20 ℃

679
680

681
682

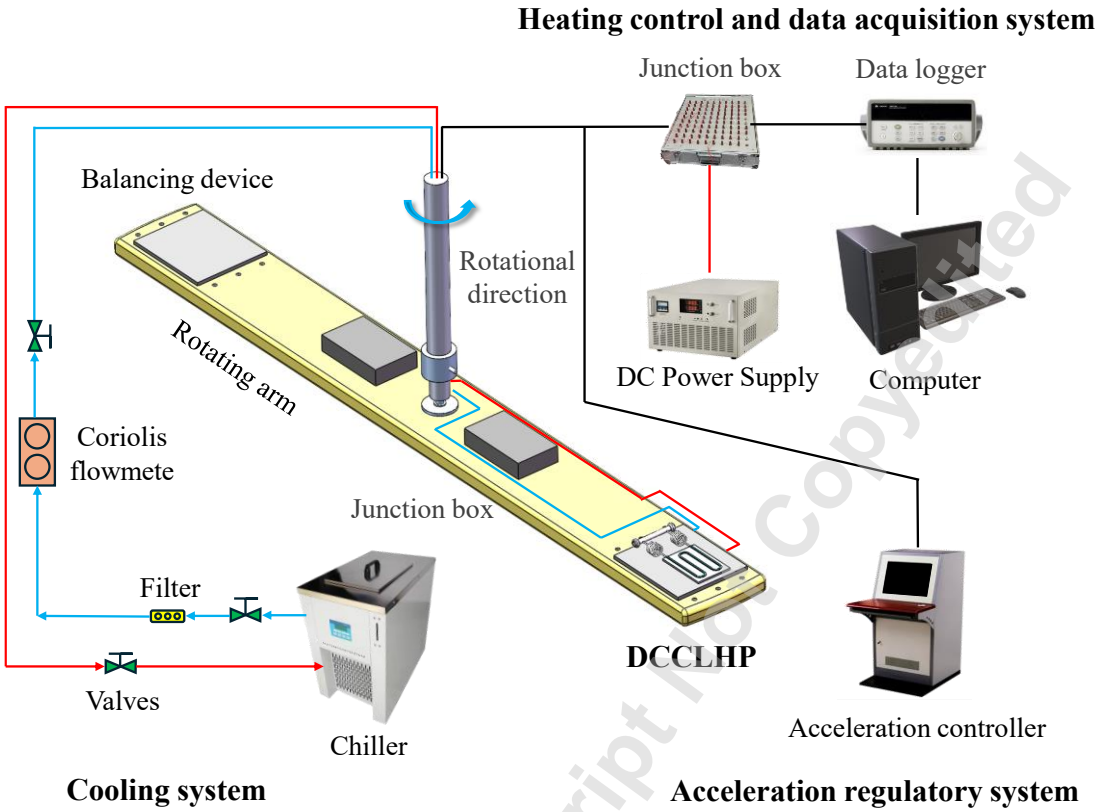

683
684

685 **Fig. 1 The schematic diagram of the experimental system**

686
687

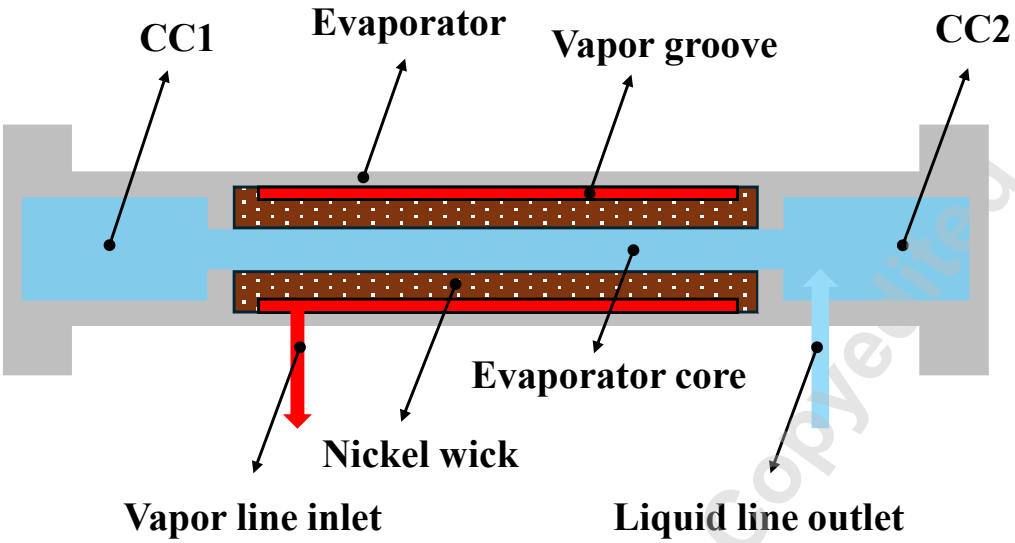

Fig. 2 Schematic diagram of the internal structure of the evaporator and CCs

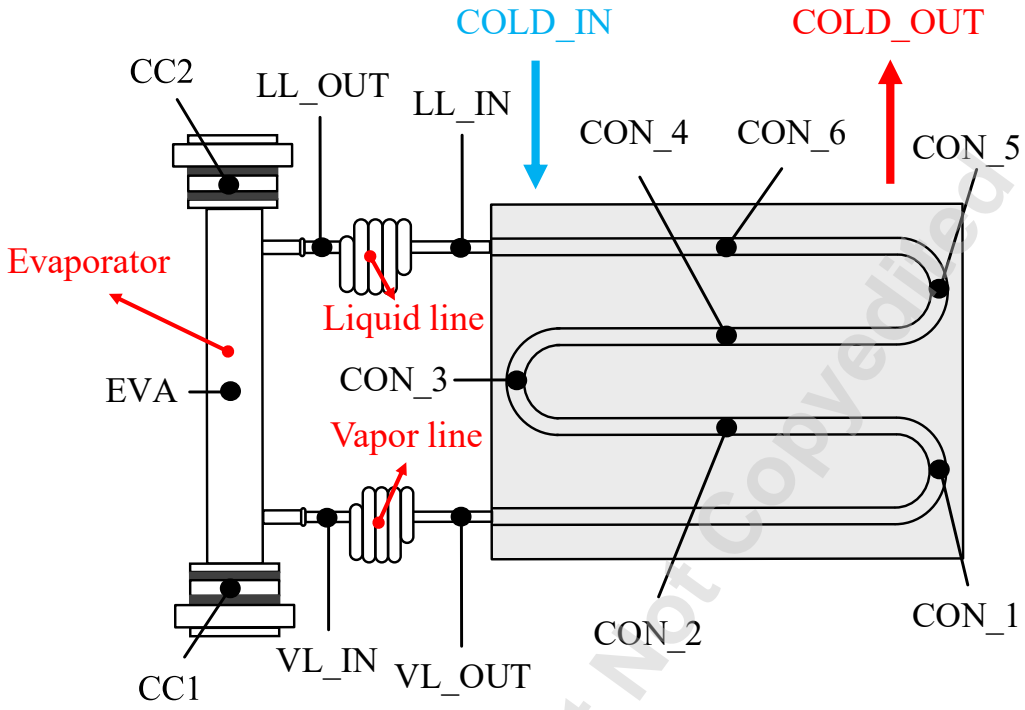

Fig. 3 Schematic diagram of temperature measurement point arrangement

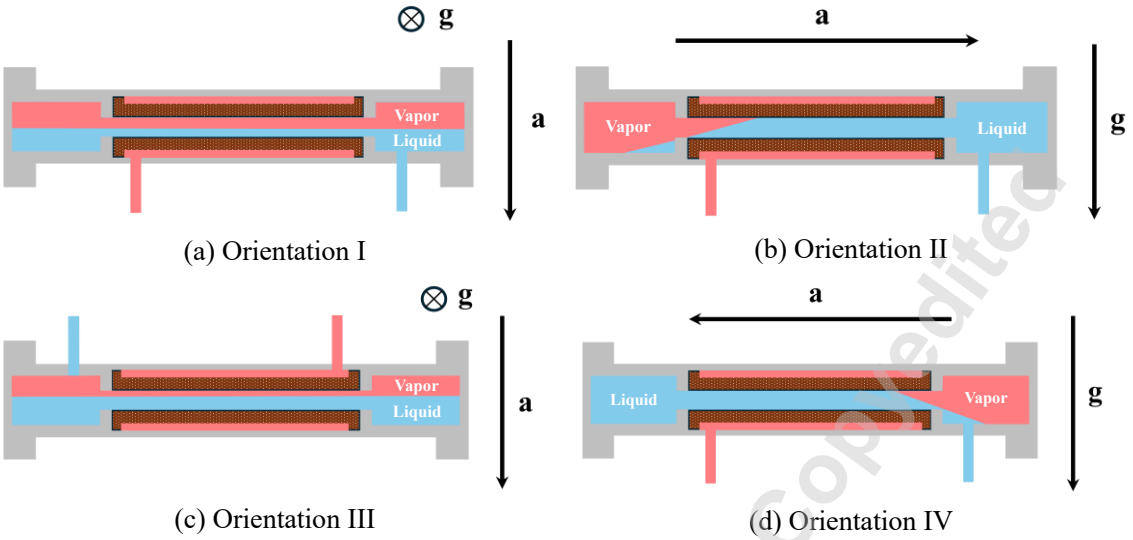

Fig. 4 Schematic diagram of installation orientations and corresponding vapor-liquid distributions

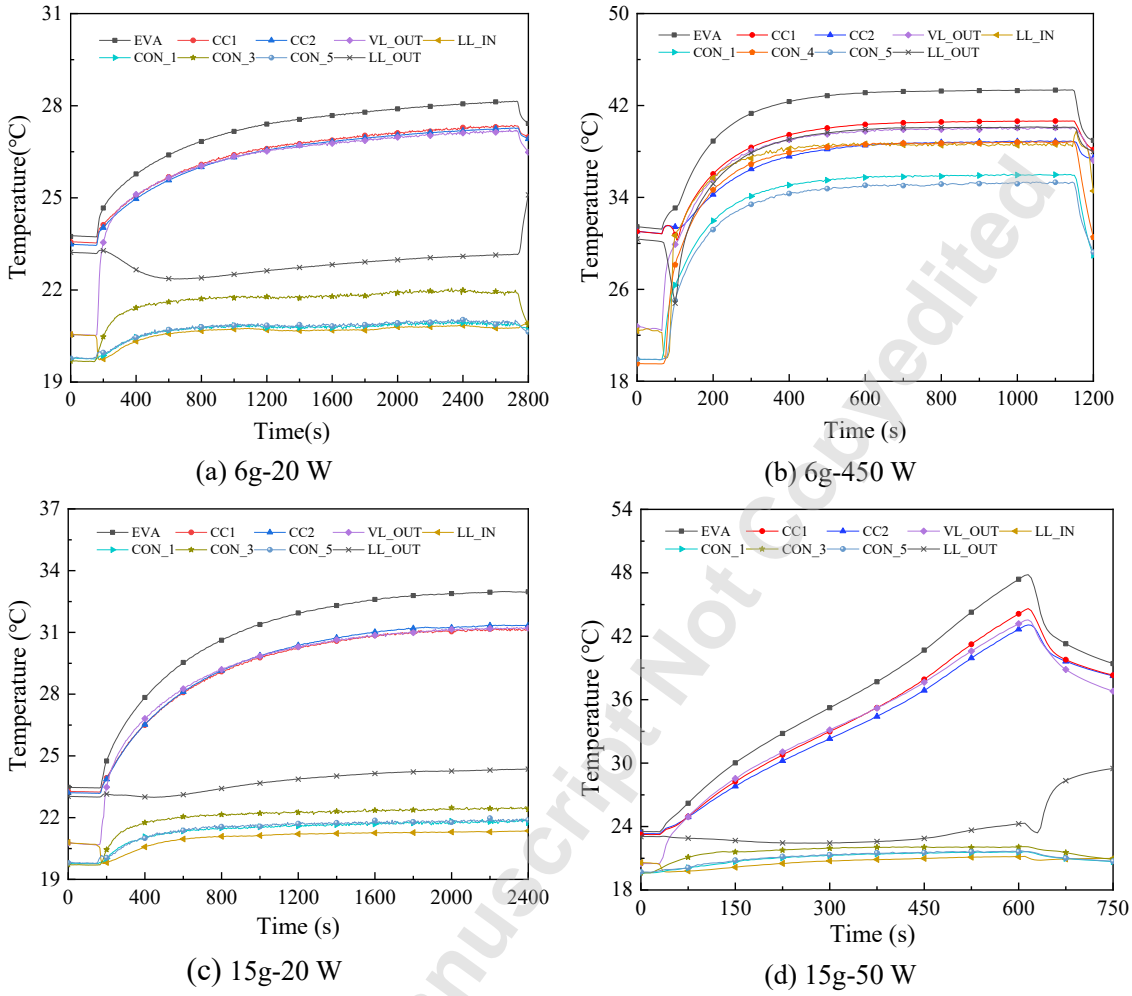

Fig. 5 Temperature variation curves of the 6g and 15g conditions at Orientation I with a heat sink temperature of 20 ℃

716
717

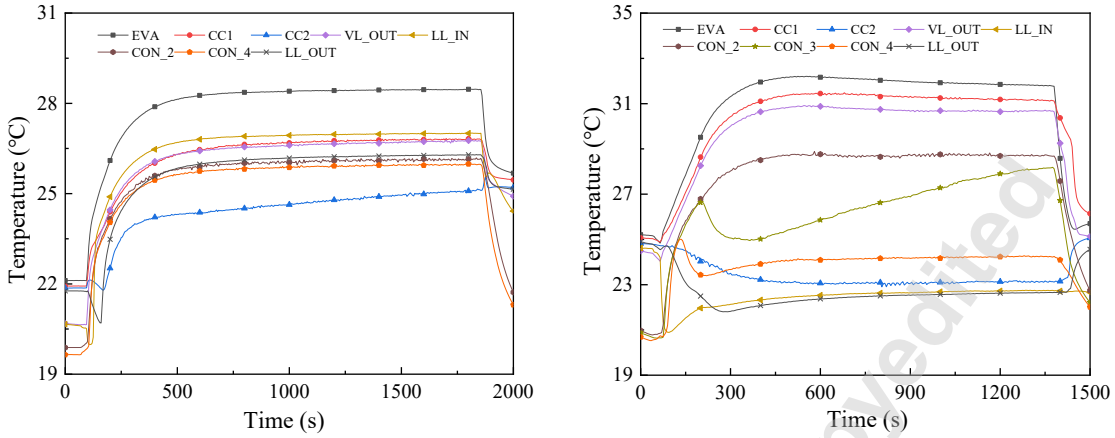

(a) 150 W-3g (b) 150 W-15g

718
719 **Fig. 6 Temperature variation curves of the 3g and 15g conditions for Orientation II at**
720 **150 W with a heat sink temperature of 20 ℃**
721
722

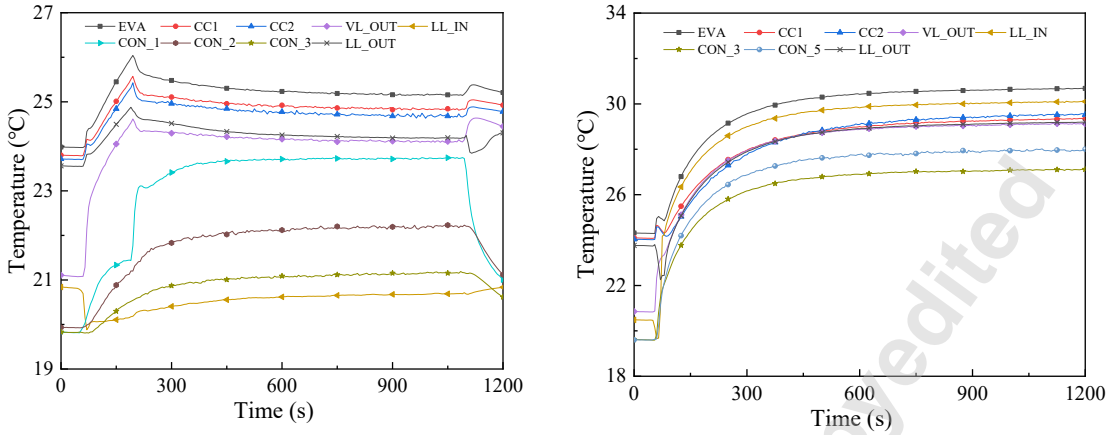

(a) 6g-30 W (b) 6g-200 W

Fig. 7 Temperature variation curves of the 6g conditions for Orientation III at 30 W and 200 W with a heat sink temperature of 20 ℃

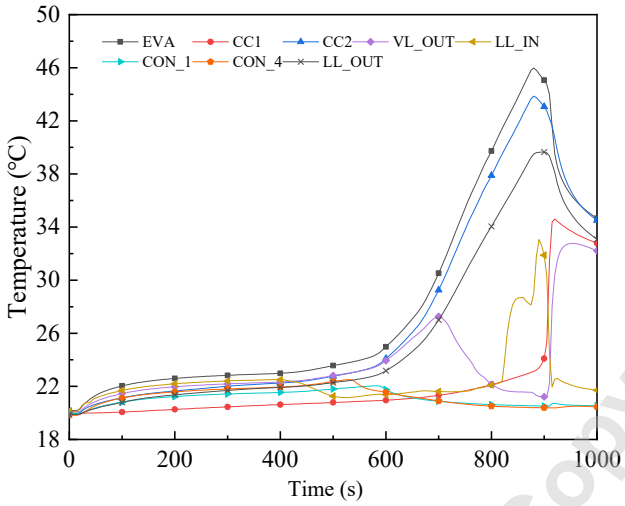

(a) 50 W

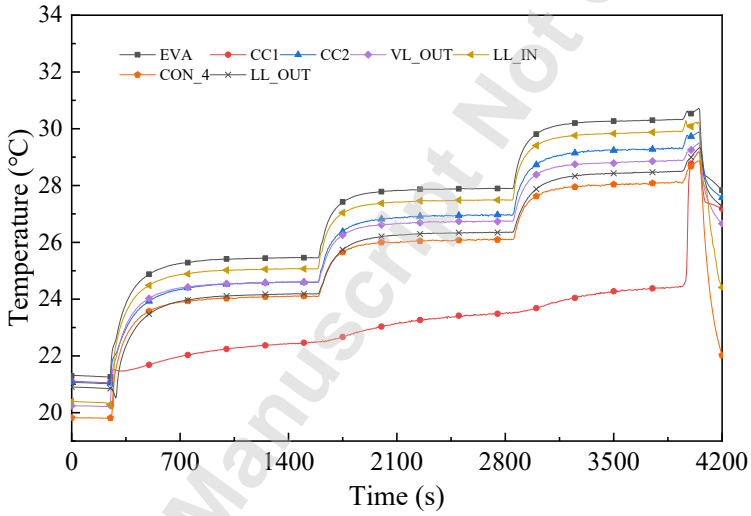

(b) 100 W-150 W-200 W

Fig. 8 Temperature variation curves of the 6g conditions at Orientation IV with a heat sink temperature of 20 ℃

741
742

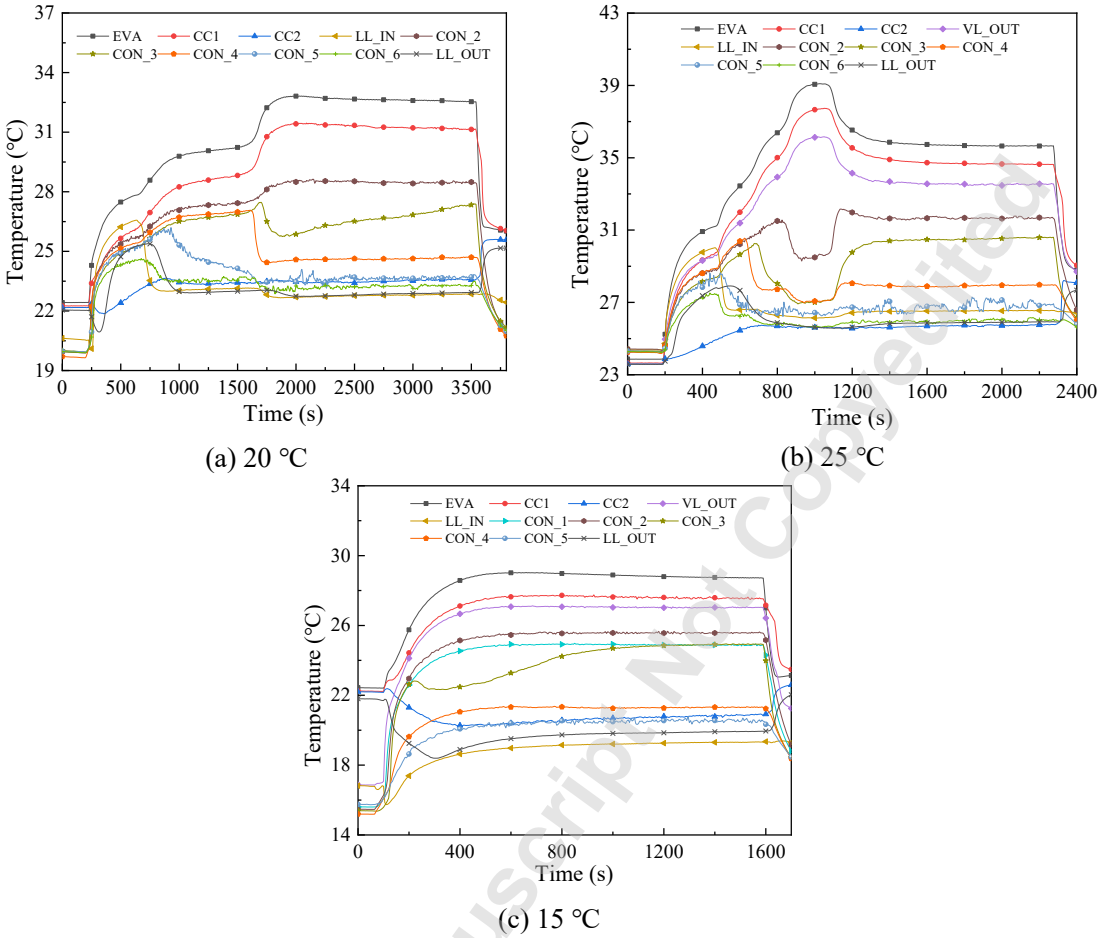

(a) 20 °C (b) 25 °C

(c) 15 °C

743
744 **Fig. 9 Temperature variation curves of the 12g and 150 W conditions at Orientation II**
745 **with different heat sink temperatures**
746
747

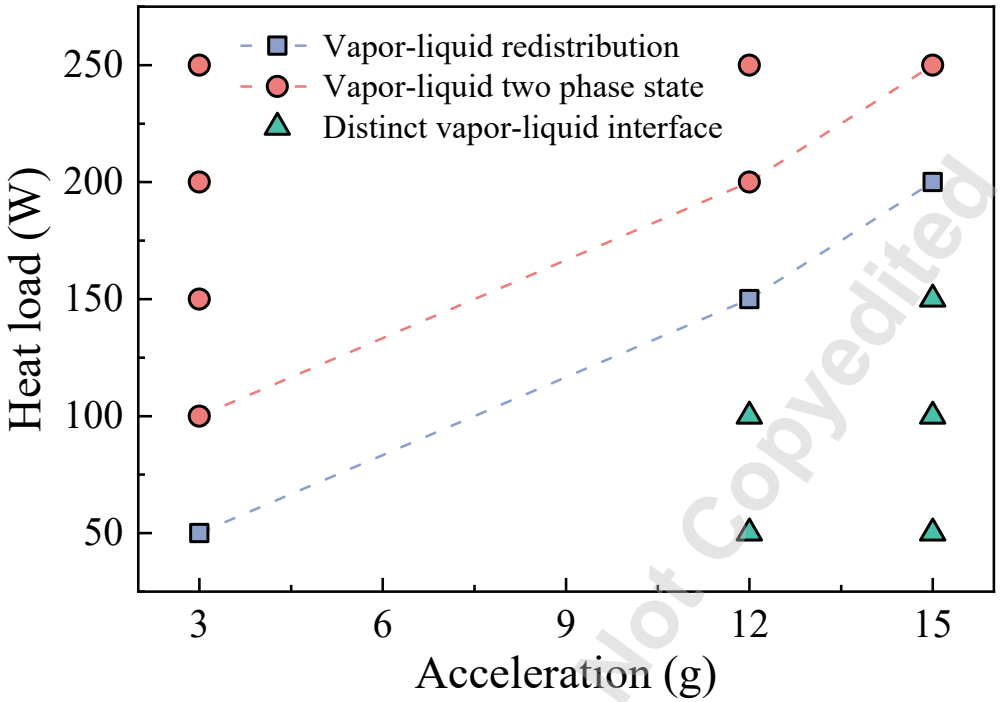

Fig. 10 Vapor-liquid distribution states of the external loop under different conditions for Orientation II with a heat sink temperature of 20 ℃

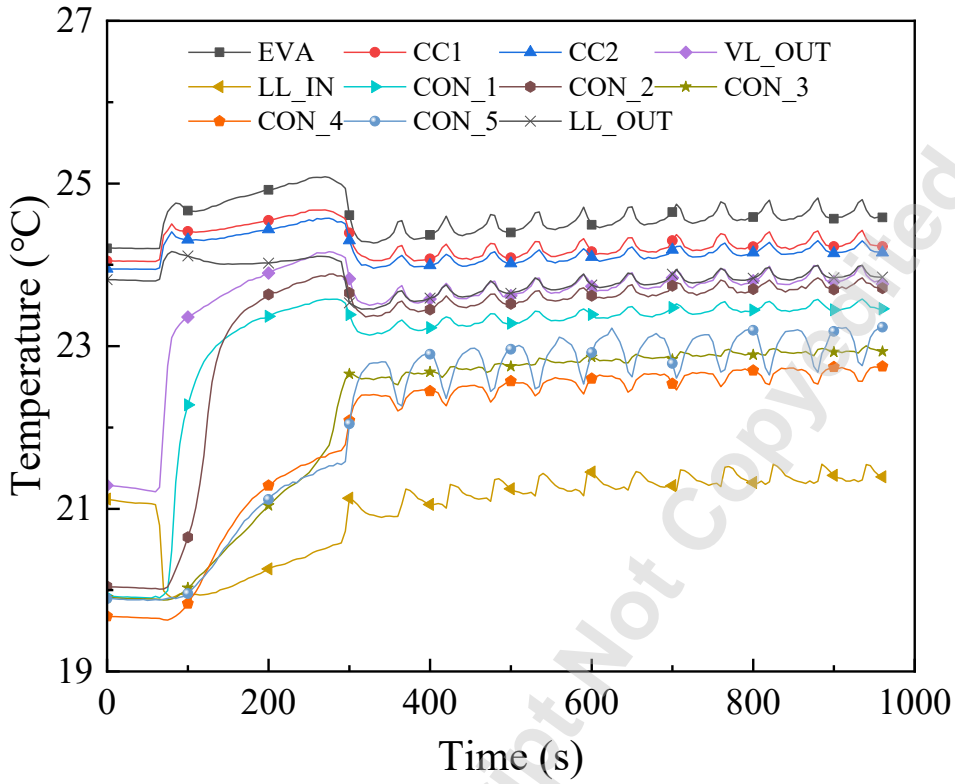

Fig. 11 Temperature oscillation curves of the DCCLHP for Orientation III at 9g and 50 W with a heat sink temperature of 20 ℃

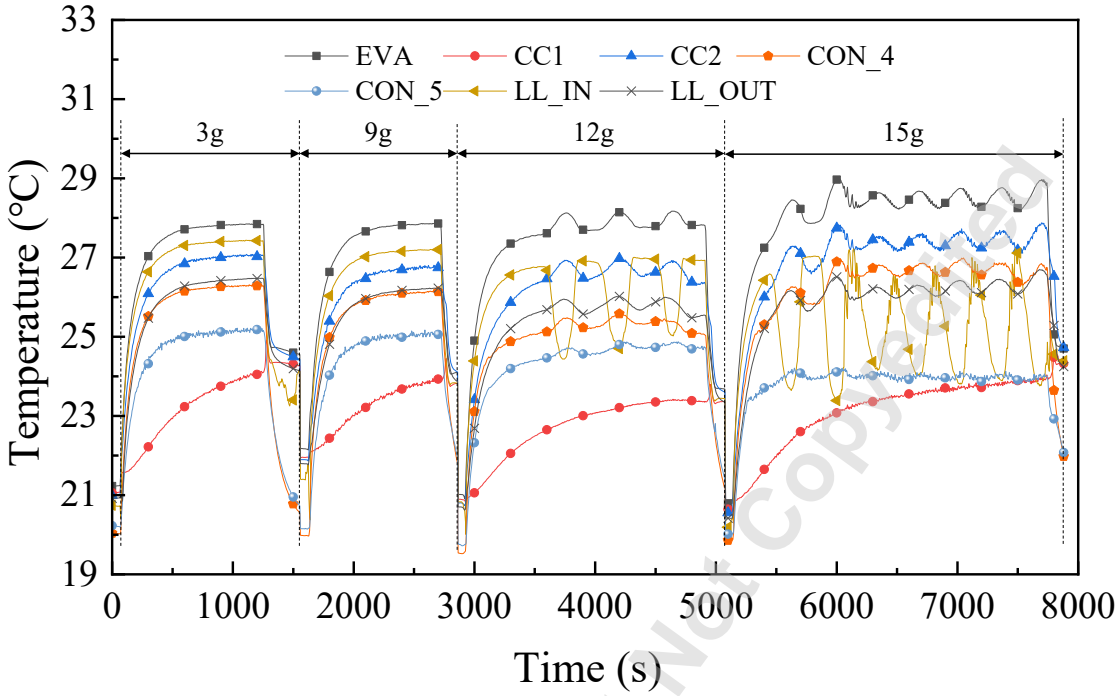

Fig. 12 Temperature variation curves of the DCCLHP for Orientation IV at 150 W with a heat sink temperature of 20 ℃ under different acceleration magnitudes

772
773

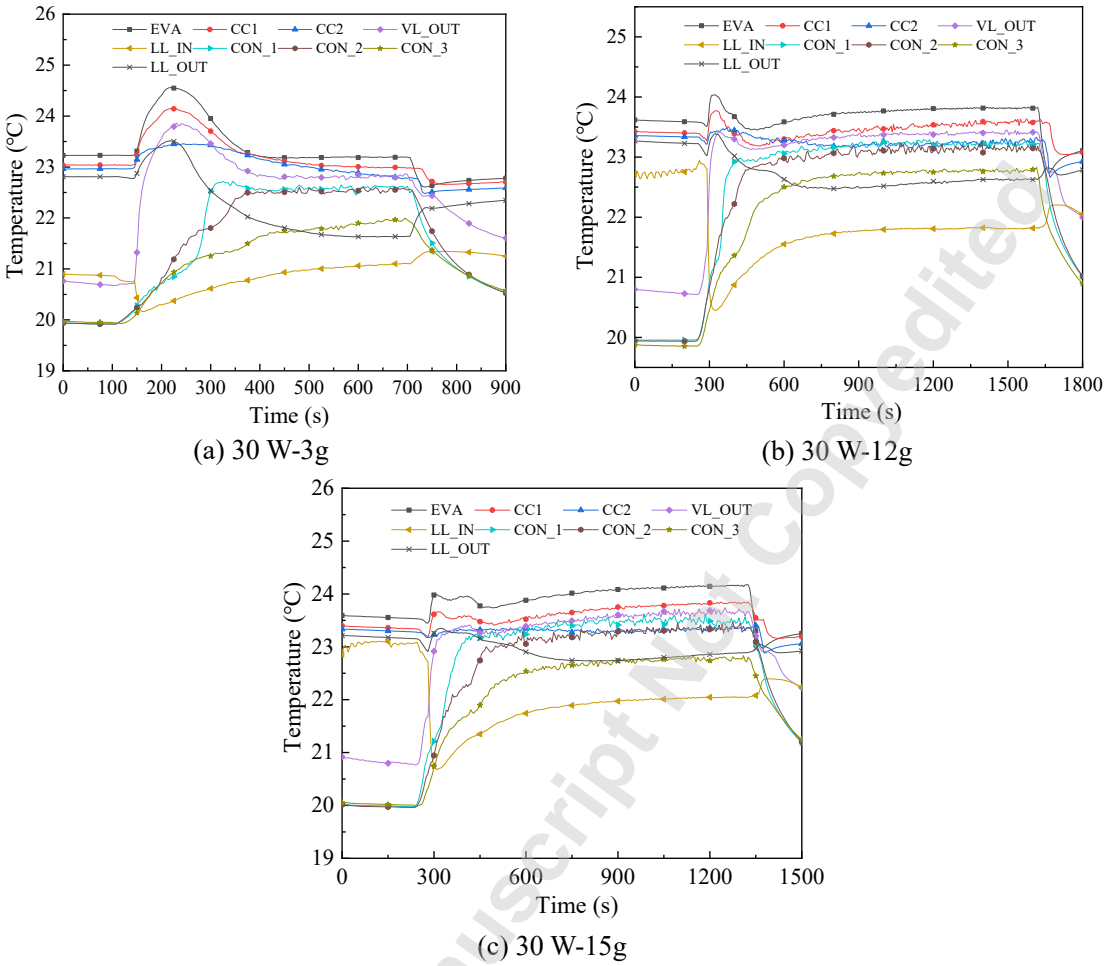

774
775 **Fig. 13 Temperature variation curves of the DCCLHP for Orientation II at 30 W with a**
776 **heat sink temperature of 20 ℃ under different acceleration magnitudes**
777
778

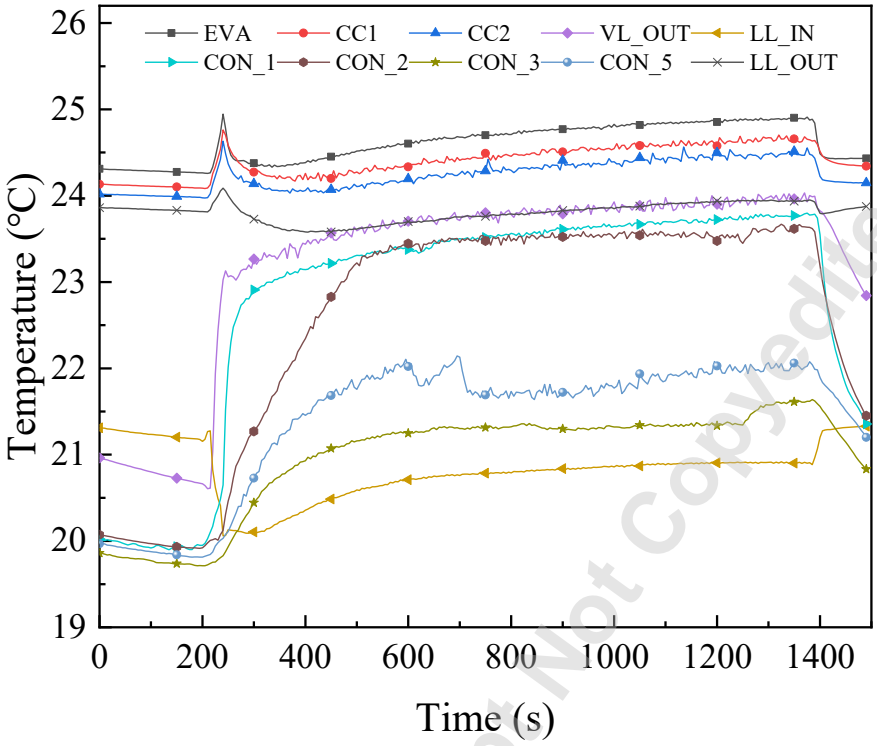

Fig. 14 Temperature variation curves of the DCCLHP for Orientation III at 30 W and 12g with a heat sink temperature of 20 ℃

787 **Table Caption List**
788

Table 1 Main design parameters of the DCCLHP

789
790
791 **Table 1 Main design parameters of the DCCLHP**
792

Components	Material	Design parameters	Dimensions
Wick	Nickel	Pore radius (μm)	0.5
		Porosity	48.5%
		Permeability (m^2)	1.3×10^{-14}
		OD/ID/Length (mm)	23/10/156
Evaporator	Stainless steel 316 L	OD/ID/Length (mm)	25/23/156
CCs	Stainless steel 316 L	OD/ID/Length (mm)	27/25/60
Liquid pipe	Stainless steel 316 L	OD/ID/Length (mm)	6/4/500
Vapor pipe	Stainless steel 316 L	OD/ID/Length (mm)	6/4/500
Condenser	Stainless steel 316 L	OD/ID/Length (mm)	6/5/1100
Working fluid	Ammonia		

793
794